ELSEVIER

Contents lists available at ScienceDirect

Optical Materials

journal homepage: www.elsevier.com/locate/optmat



BaV₂O₆·H₂O: A nonlinear optical crystal with a large bandgap

Wenqiang Chen^a, Wenyao Zhang^a, Ming-Hsien Lee^b, Qun Jing^{a,**}, Xuefang Lu^a, Zhaohui Chen^{a,*}



- ^a Physical and Chemical Detecting Center, College of Chemistry and Chemical Engineering, College of Physical Science and Technology, Xinjiang University, 666 Shengli Road, Urumqi, 830046, China
- b Department of Physics, Tamkang University, New Taipei City, 25137, Taiwan

ARTICLE INFO

Keywords: Vanadate Large bandgap Nonlinear optical material Hydrothermal method

ABSTRACT

The first Ba-containing hydrated vanadate as nonlinear optical (NLO) material, BaV₂O₆·H₂O, was synthesized by facile hydrothermal method. The single-crystal X-ray diffraction result shows that this compound crystallizes in the acentric orthorhombic space group of $P2_12_12_1$ with cell parameters a=7.3993(6) Å, b=8.9934(7) Å, and c=9.7206(8) Å. UV-vis-IR diffuse reflectance spectrum shows that the compound has a large bandgap of 4.60 eV and moderate transparency range. The title compound shows second-harmonic generation (SHG) efficiency about 0.5 times of KH₂PO₄ (KDP). The structure-property relationship of BaV₂O₆·H₂O was clarified by the first-principles studies.

1. Introduction

Nonlinear optical (NLO) materials have received extensive commercial and academic interest due to their all-round scientific and technological applications [1–7]. The materials are pivotal components of solid-state lasers, which produce coherent light from the ultraviolet (UV) to the infrared (IR) through a frequency conversion. In recent years, many outstanding NLO materials have been discovered from the UV to the IR regions [8–16]. Vanadates have attracted much attention owing to their possible applications such as optical, photoluminescence, electrical and catalytic materials [7,17,18]. The survey demonstrates that a host of good performance NLO vanadates have large SHG and wide transparency range to mid-IR. For example, $K(VO)_2O_2(IO_3)_3$ [15], $NaVO_2(IO_3)_2(H_2O)$ [18], $K_2SrVB_5O_{12}$ [19], $Zn_2(VO_4)(IO_3)$ [20], $Na_3VO_2B_6O_{11}$ [21], $A_4(VO_2)_2(SeO_3)_4(Se_2O_5)$ ($A=Sr^{2+}$ or Pb^{2+}) [22] and so on.

Since vanadium is typically observed in VO₄, VO₅, and VO₆ polyhedra coordination environments and is found in oxidation states of 2+, 3+, 4+ or 5+ [23], it can form diverse vanadium-containing new structures and own many attractive properties. Since vanadium can constitute distorted tetrahedra, pentahedra or octahedra, this polyhedron with distortion d^0 transition metals maybe generate great SHG responses. Therefore, it may promote the formation of new NLO materials through introducing d^0 transition metal V atoms. The NLO vanadates can be separated into two types: multiple vanadates, such as NaVO₂(IO₃)₂(H₂O), Na₃VO₂B₆O₁₁, K₂SrVB₅O₁₂, and so on; Vanadates

only with covalent tetrahedral VO₄ $^{3-}$, such as Li₃VO₄ [24,25], α - and β -Ag₃VO₄ [26], and so on.

So far, the majority of NLO vanadates are subjected to the main barriers that are little bandgaps and low laser damage thresholds (LDTs), which severely impede their applications. As we all known that a large bandgap maybe lead to a high LDT [25,27,28]. The increase of bandgap can availably reduce the occurrence of two-photon and multiphoton absorptions, thereby increasing LDT [29,30]. Therefore, synthesizing efficient NLO vanadates with large bandgaps is necessary and still ongoing.

It is common knowledge that combining with alkali metal or alkaline earth metal ions may enlarge bandgaps of compounds [31–37], owing to the strong ionicity of these ions that can enhance the interaction between the anionic groups and cations [38]. According to such an idea, we synthesized the first NLO material of Ba-containing hydrated vanadate by facile hydrothermal method, BaV₂O₆·H₂O. The structure of BaV₂O₆·H₂O was first reported by Ulická et al. [39]. In this paper, we focused on the comprehensive linear optical and NLO properties of the title compound. Then, theoretical studies were carried out to further deepen the comprehending of the origins of the optical properties. The compound has a moderate transparency range (0.268–2.748 μ m) and large experimental bandgap of 4.60 eV. In addition, expatiations of the paper are crystal structure, thermal analysis, elemental analysis and powder SHG measurements on BaV₂O₆·H₂O.

E-mail addresses: qunjing@xju.edu.cn (Q. Jing), chenzhaohui686@sina.cn (Z. Chen).

^{*} Corresponding author.

^{**} Corresponding author.

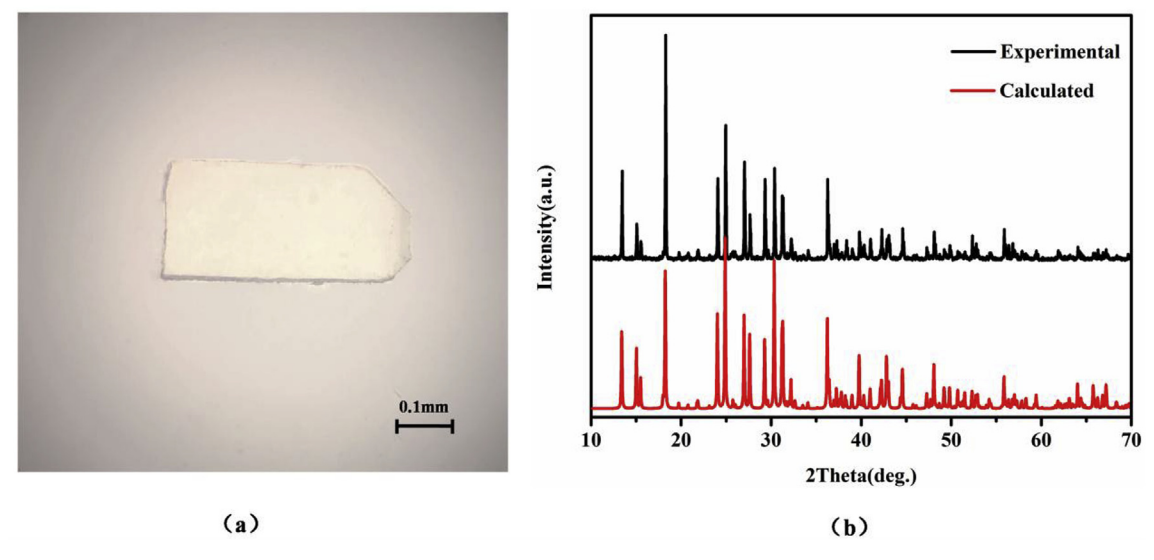


Fig. 1. (a) Photograph of BaV₂O₆·H₂O crystal. (b) Experimental and calculated XRD patterns of BaV₂O₆·H₂O.

2. Experimental section

2.1. Synthesis

Analytically pure BaCO $_3$, V $_2O_5$ and H $_3PO_4$ were available from commercial sources without further purification. BaV $_2O_6$ ·H $_2O$ was synthesized by a facile hydrothermal reaction. The mixture of BaCO $_3$ (0.5920 g, 3 mmol), V $_2O_5$ (0.3638 g, 2 mmol), H $_3PO_4$ (0.0980 g, 1 mmol) in deionised water (2 mL) was sealed in a 23 mL Teflon-lined stainless steel reactor. Then the reactor was heated to 200 °C, held at 200 °C for 3 days and cooled to 30 °C at a rate of 5 °C h $^{-1}$. Finally, colorless and transparent crystals of BaV $_2O_6$ ·H $_2O$ (Fig. 1a) were obtained, cleaned with deionised water, then air-drying overnight at room temperature. Here, H $_3$ PO $_4$ acted as the mineralizer in synthesizing BaV $_2O_6$ ·H $_2O$ crystals.

2.2. Single-crystal X-ray diffraction

Single-crystal X-ray diffraction data of BaV2O6:H2O were collected on a Bruker Smart APEX II charge-coupled device (CCD) single crystal monochromatic diffractometer (graphite $Mo-K_{\alpha}$ radiation, $\lambda = 0.71073 \,\text{Å}$) at room temperature. The SADABS program is used for the numerical absorption corrections [40]. The structure was solved by direct methods and then refined by the full-matrix least squares method with anisotropic displacement parameters in SHELXTL-97 system [41]. In addition, structure was verified with the aid of the program PLATON [42]. Relevant crystal parameters and structure refinement informations are given detailedly in Table 1. Atoms coordinates, isotropic or equivalent displacement parameters and bond valence are summarized in Table S1 in the Supporting Information (SI). Selected bond distances and angles are listed in Table S2 in the SI.

2.3. Powder X-ray diffraction

Powder X-ray Diffraction (PXRD) data were collected on a Bruker D8 Advance X-ray diffractometer with graphite-monochromatic $\text{Cu-}K_{\alpha}$ radiation ($\lambda=1.5418\,\text{Å}$). The 2θ range was $10–70^{\circ}$ with a step width of 0.02° and a fixed time of 1 s. The experimental PXRD pattern of $\text{BaV}_2\text{O}_6\text{:H}_2\text{O}$ showed agreement with the calculated one from the single crystal model (Fig. 1b).

Table 1Crystal data and structure refinement for BaV₂O₆·H₂O.

Empirical formula	BaV_2O_6 · H_2O
Formula weight	353.24
Temperature [K]	296(2)
Wavelength [Å]	0.71073
Crystal system	Orthorhombic
Space group	$P2_12_12_1$
	a = 7.3993(6) Å
Unit cell dimensions	b = 8.9934(7) Å
	c = 9.7206(8) Å
Volume [Å ³]	646.86(9)
Z	4
Calculated density [Mg/m³]	3.627
Absorption coefficient [mm ⁻¹]	8.830
F(000)	640
Crystal size [mm ³]	$0.250 \times 0.100 \times 0.050$
Theta range for data collection [°]	3.09 to 27.54
Limiting indices	$-9 \leq h \leq 9, \ -5 \leq k \leq 11,$
	$-12 \le l \le 12$
Reflections collected/unique	3891/1469 [R(int) = 0.0164]
Completeness to theta = 27.54 [%]	99.2%
Refinement method	Full-matrix least-squares on F_0^2
Data/restraints/parameters	1469/2/98
Goodness-of-fit on F _o ²	1.071
Final R indices $[F_o^2 > 2\sigma(F_o^2)]^{[a]}$	$R_1 = 0.0128, wR_2 = 0.0263$
R indices (all data) [a]	$R_1 = 0.0134, wR_2 = 0.0265$
Absolute structure parameter	0.000(16)
Extinction coefficient	0.0064(2)
Largest diff. peak and hole [e·Å ⁻³]	0.305 and -0.321

[a] $R_1 = \Sigma ||F_o||$ - $|F_c||/\Sigma |F_o||$ and $wR_2 = [\Sigma w(F_o^2 - F_c^2)^2/\Sigma wF_o^4]^{1/2}$ for $F_o^2 > 2\sigma(F_o^2)$.

2.4. Thermal analysis

Thermal gravimetric (TG) and differential scanning calorimetry (DSC) analyses were performed on a HITACHI STA 7300 thermal analyzer instrument. The crystal sample (5–10 mg) was placed in a platinum crucible and heated from 30 to 700 $^{\circ}\text{C}$ at a rate of 5 $^{\circ}\text{C}$ min $^{-1}$ under a constant flow of argon atmosphere.

2.5. Spectroscopy analysis

The optical transmission range of the compound was recorded on a UV– ν is–NIR spectrophotometer (SolidSpec-3700DUV) for the range of 190–2600 nm (0.19–2.6 μ m) and a MIR spectrophotometer (VERTEX 70) for the range of 400–4000 cm $^{-1}$ (2.5–25 μ m) with the sample

embedded in KBr matrix. Reflectance spectrum was transformed to absorbance spectrum by the following Kubelka-Munk function [43],

$$F(R) = \frac{(1-R)^2}{2R} = \frac{K}{S}$$

where *R* is the reflectance, *K* is the absorption, and *S* is the scattering.

2.6. Elemental analysis

Elemental analysis of the single crystal was carried out by using a LEO-1430VP scanning electron microscope (SEM) equipped with energy-dispersive spectroscopy (EDS). For BaV_2O_6 · H_2O , calculated: Ba, 38.88%; V, 28.84%; O, 31.71%; H, 0.57%. Found: Ba, 39.46%; V, 29.64%; O, 30.90%.

2.7. Second-harmonic generation

The second-harmonic generation (SHG) response of $BaV_2O_6\cdot H_2O$ was carried out using an improved Kurtz-Perry system [44] with a 1064 nm Q-switched Nd:YAG laser. Particulars of the equipment and methodology have been published [45,46]. In order to make relevant contrast with known SHG materials, crystalline potassium dihydrogen phosphate (KDP) and $BaV_2O_6\cdot H_2O$ samples were ground and sifted into the same particle sizes ranges.

2.8. Computational descriptions

The electronic properties were calculated by using CASTEP package [47]. The generalized gradient approximation (GGA) using Perdew-Burke-Ernzerhof (PBE) functional was chosen in the calculations [48]. On the basis of the norm-conserving pseudopotential (NCP) [49], the valence electrons of the component elements were treated as Ba $5s^25p^66s^2$, V $3d^34s^2$, O $2s^22p^4$, H $1s^1$. The kinetic energy cutoff was set at 830 eV and Monkhorst-Pack $3\times3\times3$ k-point meshes were used. The other convergent criteria and calculation parameters were the default values of the CASTEP code. According to the electronic band structure, the birefringence and refractive indices were theoretically determined [50]. The detailed calculation formulas of the SHG coefficients and refractive indices can be found elsewhere [51].

3. Results and discussion

3.1. Crystal structure

BaV2O6·H2O crystallizes in the acentric orthorhombic space group of $P2_12_12_1$ (No. 19) with cell parameters a = 7.3993(6) Å, b = 8.9934(7) Å, and c = 9.7206(8) Å. In the asymmetric units, there are one unique barium atom, two unique vanadium atoms, seven unique oxygen atoms and two unique hydrogen atoms (Fig. S1 in the SI). All V atoms are coordinated to four oxygen atoms to create the VO₄ tetrahedra. The V(1)O₄ is connected with V(2)O₄ by corner-sharing to form the V₂O₇ unit. A stretch of successive V₂O₇ units was observed to constitute the infinite twisted spiral [V₂O₆]_∞ chains by sharing O(3) and O(4) (Fig. 2a). The Ba atoms are coordinated to ten oxygen atoms to create irregular BaO_{10} polyhedra. Stretches of continuous BaO_{10} polyhedra are observed to form infinite jagged [BaO₆]_∞ chains by sharing O atoms (Fig. 2b). The [V₂O₆]_∞ and [BaO₆]_∞ chains are interlaced to form two-dimensional (2D) layers (Fig. 2c). Adjacent layers are further connected by the O atoms to form three-dimensional (3D) framework. It is two-thirds or one-third for the occupancy of H atoms in connection with O atoms, so it is hard to accurately determine the positions of H atoms. The average values of the bond valence sums for the Ba atoms, the V atoms, the O atoms and the H atoms were determined to be 2.06, 5.16, 2.08 and 1.08 (Table S1 in the SI) respectively, which are in good agreement with the ideal valences.

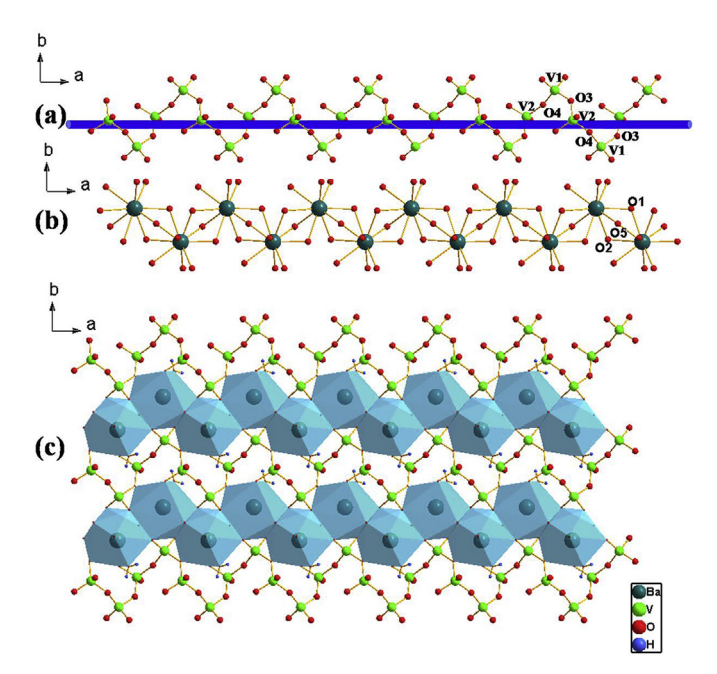


Fig. 2. The structure of $BaV_2O_6 \cdot H_2O$: (a) spiral $[V_2O_6]_{\infty}$ chain, (b) jagged $[BaO_6]_{\infty}$ chain, (c) two-dimensional layer. The BaO_8 polyhedra are show in sky blue. (For interpretation of the references to color in this figure legend, the reader is referred to the Web version of this article.)

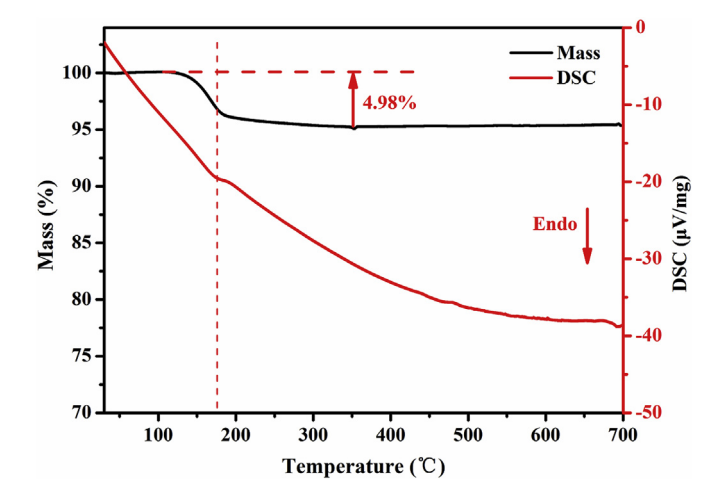


Fig. 3. TG-DSC cruves of $BaV_2O_6 \cdot H_2O$.

3.2. Thermal analysis

TG-DSC curves (Fig. 3) showed the thermal properties of Ba-V $_2{\rm O_6\cdot H_2O}$. TG studies indicated that BaV $_2{\rm O_6\cdot H_2O}$ was stable up to 120 °C. When heating was continued, the crystalline water started to decompose that ends at 350 °C. The total weight loss of 4.98% is close to computed value of 5.10% corresponding to the mass content of water molecules in the title compound.

3.3. Spectral analysis

Transparency range for BaV_2O_6 · H_2O is shown in Fig. 4. Obviously, little absorptions occur in UV–vis–NIR region; it exhibits obvious absorptions from 2.748 to 3.275 μm in mid-IR region and these peaks are connected with water, which means that hydrate water leads to minish the transparency range. Otherwise, the transparency range of the title compound will be broadened from 0.268 to 6.233 μm . Consequently, the title compound exhibits moderate transparency range from the

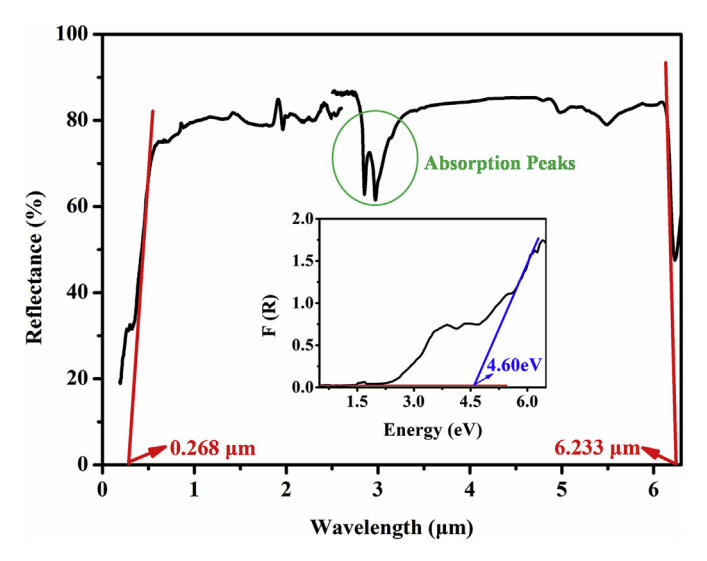


Fig. 4. The UV-vis-IR diffuse reflectance spectrum of $BaV_2O_6 \cdot H_2O$ and an approximate bandgap of 4.60 eV.

near-UV to the near-IR region (0.268–2.748 μm) and an absorption edge about 268 nm.

In the F(R)-E plot, extrapolating the linear part of the rising curve to zero provides an approximate experimental bandgap of 4.60 eV (Fig. 4). The bandgaps and LDTs of some typical IR NLO materials are listed in Table S4 in the SI. From the table we can see, the LDTs go up with the increase of bandgaps in general. The bandgap of $BaV_2O_6\cdot H_2O$ is the largest among NLO vanadates in Table 2, which indicates that the title crystal maybe lead to a high LDT. Guided by these thoughts, we are further exploring new NLO materials with large bandgaps and wide transparent range in the non-aqueous vanadates.

The IR spectrum of BaV_2O_6 · H_2O was shown in Fig. S2 in the SI exhibiting the following absorption peaks. The absorption bands range from 592 to $944\,\mathrm{cm}^{-1}$, which were assigned to the stretching and bending vibrations of the V–O and O–V–O groups. The OH $^-$ groups in the material were also clearly confirmed by the broad absorption peak centered at around 3366 and 3506 cm $^{-1}$. A strong peak at $1604\,\mathrm{cm}^{-1}$ confirms the presence of H–O–H bending mode, this means that water is contained in this compound. The results are in agreement with previous reports [23,52].

3.4. Second-harmonic generation

Due to the NCS space group, we studied the SHG properties of BaV_2O_6 : H_2O . As shown in Fig. 5, as particle sizes increases, the SHG intensity of BaV_2O_6 : H_2O increases firstly and then decreases. It is clearly shown that BaV_2O_6 : H_2O exhibits no phase-matching response and SHG intensity is the largest in the particle size range of $88-105\,\mu m$. Therefore, the SHG efficiency of BaV_2O_6 : H_2O is about 0.5 times of KDP.

Table 2Bandgaps and LDTs comparison with some NLO vanadates.

Compounds	E _g (eV) ^[b]	LDT (MW/cm ²)
$Zn_2(VO_4)(IO_3)$	2.26	_
$K(VO)_2O_2(IO_3)_3$	2.66	-
$Na_3VO_2B_6O_{11}$	3.35	-
$K_2SrVB_5O_{12}$	4.13	-
Li ₃ VO ₄	4.27	125.5
$BaV_2O_6 \cdot H_2O$	4.60	-

[b] Eg is the experimental bandgap.

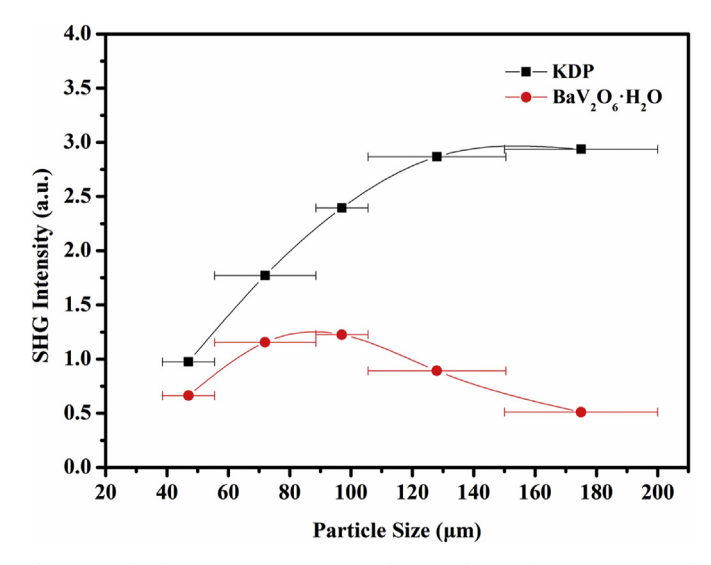


Fig. 5. Result of power SHG intensity on the particle size for $\rm BaV_2O_6\cdot H_2O$ and KDP samples.

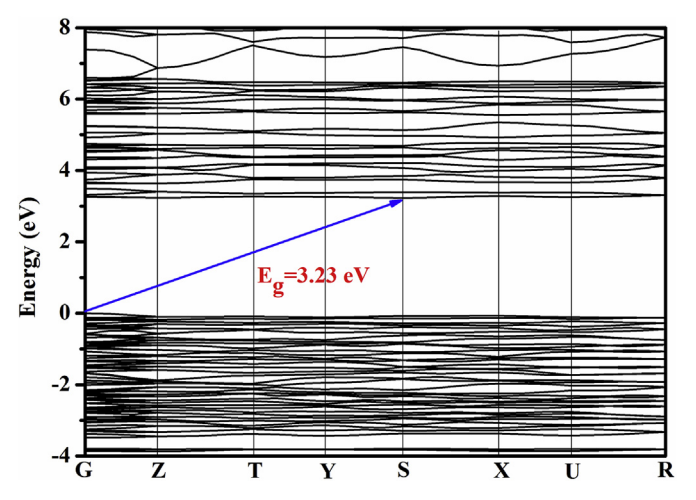


Fig. 6. The electronic band structure of BaV₂O₆·H₂O.

3.5. Electronic structure calculation

Following the method described above, the electronic band structure of BaV_2O_6 - H_2O was analyzed. As shown in Fig. 6, the valence band (VB) maximum is found at the G point, and the conduction band (CB) minimum is found at the S point, manifesting that it is an indirect bandgap compound. The calculated bandgap of 3.23eV is slightly smaller than the experimental value of 4.60 eV, which may have relation with the derivative discontinuity of the exchange-correlation energy [53].

In order to further comprehend the electronic structure and structure-property relationships, the projected density of states (PDOS) of title compound was calculated using Gaussian broadening method with smearing width 0.01 eV. The obtained PDOS is shown in Fig. 7. As shown in Fig. 7, there are isolated Ba-p states (nearby $-9.5\,\mathrm{eV}$), the hybrid V—O states and the H-s states (nearby $-8\,\mathrm{eV}$) at the energy range from -10 to Fermi level. The states at the top of valence band (from $-4\,\mathrm{eV}$ to Fermi level) are mainly from the O-p states and the V-d states, then for the bottom of conduction band the states are also mainly from the O-p states and V-d states. As we all know that the optical properties are determined by electron transition nearby the Fermi level, therefore authors believe that the VO₄ groups have a major role in deciding refractive indices, birefringence and SHG response. The arrangement of the V(1)O₄ and V(2)O₄ groups is shown in Fig. S3 in the

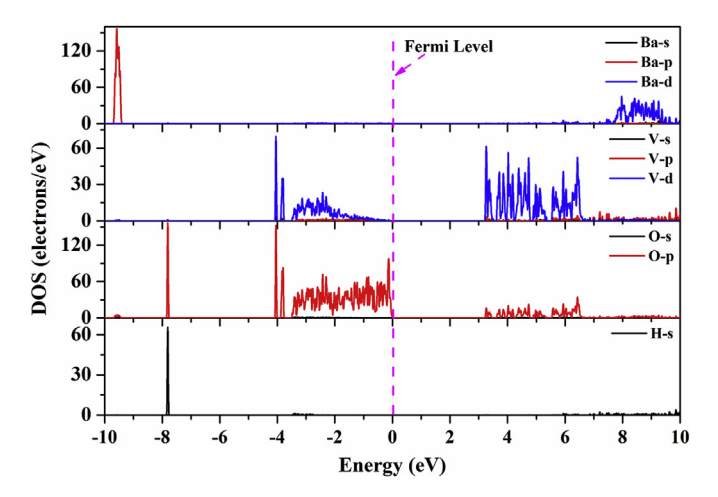


Fig. 7. The projected density of states (PDOS) of $BaV_2O_6 \cdot H_2O$.

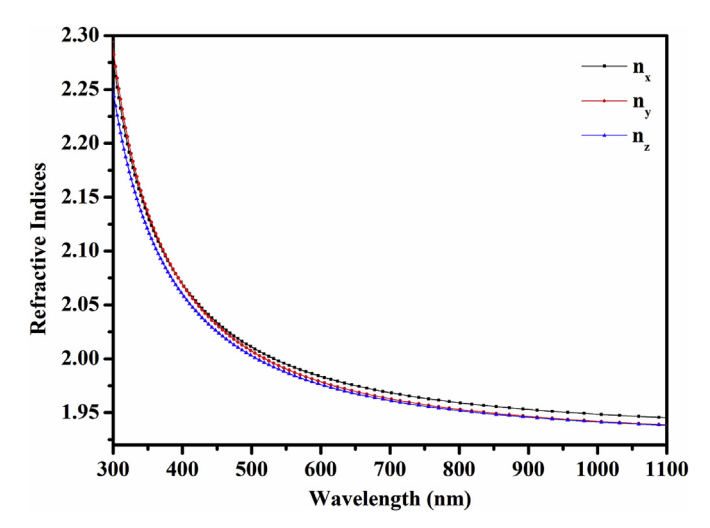


Fig. 8. The calculated refractive indices of BaV₂O₆·H₂O.

SI. The arrangement of the $V(1)O_4$ groups is roughly the same direction along the a axis, whereas the interdigitated $V(2)O_4$ groups are arranged in opposite directions each other. Therefore, the macroscopic polarity of the compound almost comes from $V(1)O_4$ groups, which maybe the main factor leading to small SHG effect of the compound.

The refractive indices and the birefringence of the title compound are also calculated. The obtained refractive indices along different optical axis are shown in Fig. 8. The $BaV_2O_6\text{-}H_2O$ crystallizes in orthorhombic crystal system $P2_12_12_1$ space group, hence it should be biaxial crystal. As shown in Fig. 8 the obtained refractive indices along x, y and z axis are about 1.94–2.28 at 300–1100 nm. One can also find out that the obtained birefringence is very small due to the similar values of n_{xv} , n_{yv} , and n_{zv} . The relative smaller birefringence made that $BaV_2O_6\text{-}H_2O$ is not phase-matchable, which is also coincided with the result of SHG research.

Using the refractive indices obtained by the first principles method, the SHG efficiency of BaV_2O_6 · H_2O was further roughly evaluated according to Eq. 18 shown in Ref. [44] $(0.5[(n^2-1)/(n+1)]^6(l_c/10)^2)$. The obtained SHG efficiency of BaV_2O_6 · H_2O is about 0.44 times that of KDP compound, which is in good agreement with the experimental value (about 0.5 times of KDP compound).

4. Conclusion

To summarize, we have successfully synthesized the first NLO material of Ba-containing hydrated vanadate BaV₂O₆·H₂O by a

straightforward hydrothermal method. According to the optical properties and calculated electronic structures, the title compound shows moderate transparent range and a large bandgap of 4.60 eV, which implies that it may exhibit high LDT. Moreover, the SHG efficiency of the crystal is illustrated by theoretical calculation and structural analysis. Guided by the conclusions, we are carrying out exploring new NLO materials with large bandgaps, phase-matching conditions and wide transparent range among the vanadates.

Declaration of interests

The authors declare that they have no known competing financial interests or personal relationships that could have appeared to influence the work reported in this paper.

The authors declare the following financial interests/personal relationships which may be considered as potential competing interests.

Acknowledgements

This work is supported by the Natural Science Foundation of Xinjiang Uygur Autonomous Region of China (Grant 2018D01C045).

Appendix A. Supplementary data

Supplementary data to this article can be found online at https://doi.org/10.1016/j.optmat.2018.12.043.

References

- [1] C.T. Chen, Y.B. Wang, B.C. Wu, K.C. Wu, W.L. Zeng, L.H. Yu, Nature 373 (1995) 322–324.
- [2] Z.G. Xia, K.R. Poeppelmeier, Acc. Chem. Res. 50 (2017) 1222-1230.
- [3] K.M. Ok, E.O. Chi, P.S. Halasyamani, Chem. Soc. Rev. 35 (2006) 710-717.
- [4] H.W. Yu, W.G. Zhang, J.S. Young, J.M. Rondinelli, P.S. Halasyamani, Adv. Mater. 27 (2015) 7380–7385.
- $\begin{tabular}{ll} [5] & Y. Wang, S.L. Pan, Coord. Chem. Rev. 323 (2016) 15-35. \end{tabular}$
- [6] G.Q. Shi, Y. Wang, F.F. Zhang, B.B. Zhang, Z.H. Yang, X.L. Hou, S.L. Pan, K.R. Poeppelmeier, J. Am. Chem. Soc. 139 (2017) 10645–10648.
- [7] C.L. Hu, J.G. Mao, Coord. Chem. Rev. 288 (2015) 1-17.
- [8] S.G. Zhao, P.F. Gong, S.Y. Luo, L. Bai, Z.S. Lin, Y.Y. Tang, Y.L. Zhou, M.C. Hong, J.H. Luo, Angew. Chem. Int. Ed. 54 (2015) 4217–4221.
- [9] Y. Wang, B.B. Zhang, Z.H. Yang, S.L. Pan, Angew. Chem. Int. Ed. 57 (2018) 2150–2154.
- [10] X.Y. Dong, Q. Jing, Y.J. Shi, Z.H. Yang, S.L. Pan, K.R. Poeppelmeier, J. Young, J.M. Rondinelli, J. Am. Chem. Soc. 137 (2015) 9417–9422.
- [11] K. Wu, Z.H. Yang, S.L. Pan, Angew. Chem. Int. Ed. 55 (2016) 6713-6715.
- [12] W.L. Yin, K. Feng, W.Y. Hao, J.Y. Yao, Y.C. Wu, Inorg. Chem. 51 (2012) 5839–5843.
- [13] P. Yu, L.J. Zhou, L. Chen, J. Am. Chem. Soc. 134 (2012) 2227–2235.
- [14] B.P. Yang, C.L. Hu, X. Xu, C. Huang, J.G. Mao, Inorg. Chem. 52 (2013) 5378–5384.
- [15] C.F. Sun, C.L. Hu, X. Xu, B.P. Yang, J.G. Mao, J. Am. Chem. Soc. 133 (2011) 5561–5572.
- [16] L. Kang, M.L. Zhou, J.Y. Yao, Z.S. Lin, Y.C. Wu, C.T. Chen, J. Am. Chem. Soc. 137 (2015) 13049–13059.
- [17] R.E. Sykora, K.M. Ok, P.S. Halasyamani, D.M. Wells, T.E. Albrecht-Schmitt, Chem. Mater. 14 (2002) 2741–2749.
- [18] B.P. Yang, C.L. Hu, X. Xu, C.F. Sun, J.H. Zhang, J.G. Mao, Chem. Mater. 22 (2010) 1545–1550.
 [19] S.J. Chen, S.L. Pan, W.W. Zhao, H.W. Yu, H.P. Wu, Z.H. Yang, Y. Yang, Dalton
- Trans. 41 (2012) 9202–9208. [20] B.P. Yang, C.L. Hu, X. Xu, C. Huang, J.G. Mao, Inorg. Chem. 52 (2013) 5378–5384.
- [21] X.Y. Fan, S.L. Pan, X.L. Hou, X.L. Tian, J. Han, J. Haag, K.R. Poeppelmeier, Cryst. Growth Des. 10 (2010) 252–256.
- [22] J. Yeon, S.H. Kim, S.D. Nguyen, H. Lee, P.S. Halasyamani, Inorg. Chem. 51 (2011) 609–619.
- [23] Z.H. Chen, Y.Q. Liu, Y.J. Shi, W.Y. Zhang, Q. Jing, Y. Fang, X.Y. Dong, New J. Chem. 41 (2017) 6730–6735.
- [24] R.D. Shannon, C. Calvo, J. Solid State Chem. 6 (1973) 538-549.
- [25] Z.H. Chen, Z.Z. Zhang, X.Y. Dong, Y.J. Shi, Y.Q. Liu, Q. Jing, Cryst. Growth Des. 17 (2017) 2792–2800.
- [26] V. Cloet, A. Raw, K.R. Poeppelmeier, G. Trimarchi, H. Peng, J. Im, A.J. Freeman, N.H. Perry, T.O. Mason, A. Zakutayev, P.F. Ndione, D.S. Ginley, J.D. Perkins, Chem. Mater. 24 (2012) 3346–3354.
- [27] H. Lin, L. Chen, L.J. Zhou, L.M. Wu, J. Am. Chem. Soc. 135 (2013) 12914–12921.
- [28] B.P. Abbott, R. Abbott, R. Adhikari, P. Ajith, B. Allen, G. Allen, R.S. Amin, S.B. Anderson, W.G. Anderson, M.A. Araya, Rep. Prog. Phys. 72 (2009) 076901.
- [29] L. Kang, D.M. Ramo, Z.S. Lin, P.D. Bristowe, J.G. Qin, C.T. Chen, J. Mater. Chem. C 1 (2013) 7363–7370.

- [30] H.M. Liu, Q. Wu, X.X. Jiang, Z.S. Lin, X.G. Meng, X.G. Chen, J.G. Qin, Angew. Chem. Int. Ed. 56 (2017) 9492–9496.
- [31] X.F. Wang, Y. Wang, B.B. Zhang, F.F. Zhang, Z.H. Yang, S.L. Pan, Angew. Chem. Int. Ed. 56 (2017) 14119–14123.
- [32] J.H. Liao, G.M. Marking, K.F. Hsu, Y. Matsushita, M.D. Ewbank, R. Borwick, P. Cunningham, M.J. Rosker, M.G. Kanatzidis, J. Am. Chem. Soc. 125 (2003) 9484–9493
- [33] K. Wu, B.B. Zhang, Z.H. Yang, S.L. Pan, J. Am. Chem. Soc. 139 (2017) 14885–14888.
- [34] X. Lin, G. Zhang, N. Ye, Cryst. Growth Des. 9 (2009) 1186-1189.
- [35] K. Feng, L. Kang, Z.S. Lin, J.Y. Yao, Y.C. Wu, J. Mater. Chem. C 2 (2014) 4590–4596.
- [36] H.W. Yu, H.P. Wu, S.L. Pan, Z.H. Yang, X. Su, F.F. Zhang, J. Mater. Chem. 22 (2012) 9665–9670.
- [37] H.P. Wu, S.L. Pan, K.R. Poeppelmeier, H.Y. Li, D.Z. Jia, Z.H. Chen, X.Y. Fan, Y. Yang, J.M. Rondinelli, H.S. Luo, J. Am. Chem. Soc. 133 (2011) 7786–7790.
- [38] Y. Huang, X.G. Meng, P.F. Gong, L. Yang, Z.S. Lin, X.G. Chen, J.G. Qin, J. Mater. Chem. C 2 (2014) 4057–4062.
- [39] L. Ulická, F. Pavelcík, K. Huml, Acta Crystallogr. A 43 (1987) 2266-2268.
- [40] SAINT-Plus, version 6.02A, Bruker Analytical X-Ray Instruments, Inc. Madison, WI,

- [41] G.M. Sheldrick, SHELXTL, Version 6.14, Bruker Analytical X-ray Instruments, Inc. Madison.
- [42] A.L. Spek, J. Appl. Crystallogr. 36 (2003) 7-13.
- [43] P. Kubelka, Z. tech. Phys. 12 (1931) 593-601.
- [44] S.K. Kurtz, T.T. Perry, J. Appl. Phys. 39 (1968) 3798–3813.
- [45] H.P. Wu, H.W. Yu, Z.H. Yang, X.L. Hou, S.L. Pan, X. Su, K.R. Poeppelmeier, J.M. Rondinelli, J. Am. Chem. Soc. 135 (2013) 4215–4218.
- [46] B.B. Zhang, G.Q. Shi, Z.H. Yang, F.F. Zhang, S.L. Pan, Angew. Chem. Int. Ed. 56 (2017) 3916–3919.
- [47] S.J. Clark, M.D. Segall, C.J. Pickard, P.J. Hasnip, M.J. Probert, K. Refson, M.C. Payne, Z. Kristallogr. 220 (2005) 567–570.
- [48] J.P. Perdew, K. Burke, M. Ernzerhof, Phys. Rev. Lett. 77 (1996) 3865-3868.
- [49] A.M. Rappe, K.M. Rabe, E. Kaxiras, J.D. Joannopoulos, Phys. Rev. B 41 (1990) 1227–1230.
- [50] Q. Jing, X.Y. Dong, X.L. Chen, Z.H. Yang, S.L. Pan, C. Lei, Chem. Phys. 453 (2015) 42–46.
- [51] Q. Jing, X.Y. Dong, Z.H. Yang, S.L. Pan, B.B. Zhang, X.C. Huang, M.W. Chen, J. Solid State Chem. 219 (2014) 138–142.
- [52] Y.Q. Liu, Z.H. Chen, Z.Z. Zhang, Y. Wang, X.Y. Dong, Z.H. Yang, Mater. Res. Bull. 83 (2016) 423–427.
- [53] J.P. Perdew, M. Levy, Phys. Rev. Lett. 51 (1983) 1884-1887.